Journal of Power Sources 205 (2012) 48–56

Contents lists available at SciVerse ScienceDirect

Journal of Power Sources

journal homepage: www.elsevier.com/locate/jpowsour

Two-dimensional charge transfer and space charge effects in extended surface solid oxide fuel cell electrodes

George J. Nelson, Brice N. Cassenti, Aldo A. Peracchio, Wilson K.S. Chiu*

HeteroFoaM Center, a DOE Energy Frontier Research Center, Department of Mechanical Engineering, University of Connecticut, 191 Auditorium Road, Storrs, CT 06269-3139, United States

ARTICLE INFO

Article history:
Received 8 September 2011
Received in revised form
20 December 2011
Accepted 1 January 2012
Available online 21 January 2012

Keywords:
Solid oxide fuel cell
Heterogeneous functional materials
Transport phenomena
Electrode microstructure

ABSTRACT

The microstructural morphology of solid oxide fuel cell electrodes has been noted to impact electrode performance, particularly with respect to charge transfer. Drawing on thermal fin analysis, an analytical modeling concept has been applied to charge transport within the SOFC electrode microstructure. This approach has the ability to account for variable cross-section solid geometry and replicates experimentally observed behavior related to SOFC electrode sintering quality. Microstructural geometries simulated by periodic structures composed of iterated base units with variable cross-section are investigated using two approaches: an axisymmetric one-dimensional analytical model and an axisymmetric two-dimensional finite element model. The one-dimensional analytical approach can account for the role of microstructural geometry without space charge effects that arise at particle contacts within the microstructure. The finite element model has been developed to enable consideration of the effects of two-dimensional transport and space charge regions near particle contact points. This more detailed model is used to benchmark the one-dimensional axisymmetric approach. Comparison of the one-dimensional and two-dimensional results demonstrates the predictive capabilities of the simplified approach.

1. Introduction

Solid oxide fuel cell (SOFC) electrodes are composite systems containing phases that fulfill multiple transport roles, with solid phases supporting charge (ion and electron) transport and an open pore phase supporting transport of gaseous products and reactants. The electrochemical reactions within SOFC electrodes are supported in part by ionic transport in the solid ion conducting phase extending from the electrolyte layer that separates the anode and cathode. The morphology and interparticle contact geometry of this phase can directly impact cell performance, particularly with respect to cell polarization losses [1–7].

Electrochemistry and charge transport in SOFC electrode microstructures have been explored using extended surface (fin) models, with existing models applying charge transport equations that are similar to the governing equation for a constant cross-section thermal fin [3,5,6,8–11]. Initial explorations of SOFC performance using fin equations were performed using a thin film approach adapted from models of electrode operation in liquid electrolyte fuel cells [1,2]. Treating the electrolyte phase as a thin film lining the pores of the electrode, Kenjo et al. demonstrated electrode types for which the thin film model is insufficient, limits for polarization resistance based on electrode thickness, and the benefits of increased electrode thickness with respect to reducing polarization resistance. This model was fit to experimental data using a lumped transport parameter that accounted for charge transfer resistance, ohmic resistance, and microstructural geometry. It was found that electrodes composed of less sinterable materials demonstrated poorer performance, with reduced performance being linked to point contacts between particles and reduced connectivity within the electrode microstructure [1]. Improved performance was seen in electrodes with well-connected $LaMnO_3$ particle clusters achieved using higher sintering temperatures [2]. These results suggest that sintering and particle contact can significantly influence electrode performance.

The thin film approach has been further modified in later electrode charge transport models, with emphasis placed on the analysis of solid phase charge transport [3–6,8–11]. Treating the electrocatalyst as a thin film coating the electrolyte, Tanner et al. [8] investigated ionic transport in a constant cross-section extended surface of electrolyte material. This model incorporated the electrode porosity and the thickness of the electrode and electrolyte regions and demonstrated the benefits of thicker electrodes in terms of reducing effective charge transfer resistance. Costamagna

* Corresponding author. Tel.: +1 860 486 3647; fax: +1 860 486 5088.
E-mail address: wchiu@engr.uconn.edu (W.K.S. Chiu).

0378-7753/$ – see front matter © 2012 Elsevier B.V. All rights reserved.
doi:10.1016/j.jpowsour.2012.01.009

Nomenclature

A	area, m^2
A_f	total fin surface area, m^2
a	slope of variable cross-section fin profile
i	current, A
L	length of fin segment, m
L_f	total fin length or electrode thickness, m
R_{ct}	charge transfer resistance, Ω-m^2
r	fin radius, m
V	voltage, V
x	spatial coordinate for fin geometry, m

Greek

η_f	fin efficiency
σ	conductivity, $S\,m^{-1}$
φ	potential difference, V

Subscripts

b	quantity evaluated at fin base
c	quantity related to fin cross-section
eff	effective
io	ionic
s	quantity related to fin surface
t	quantity evaluated at fin tip
tot	total

et al. [3,4] formulated and solved an ordinary differential equation comparable to the fin equation that described overpotential in an electrode composed of packed spheres, accounting for the ionic and electronic phases. The effects of bulk electrode thickness and composition in relation to percolation thresholds and particle sizes were considered. In addition to the work of Costamagna et al. [3,4], several models have applied percolation theory to study the impact of microstructure on SOFC transport phenomena [5,6,9–14]. Such models typically require either the application of effective conductivities [9,10,12] or the numerical solution of random resistance networks [5,6,13,14]. More detailed interparticle contact geometry has been addressed by Zhao and Virkar [7] through the development of analytical expressions for the resistivity of porous electrodes. It was found that porous electrode resistivity decreased as sintering temperatures and times were increased. This performance improvement was shown to be the result of broader interparticle necks formed at higher temperatures and longer treatment times, which were observed in scanning electron microscope images. A key factor in the analytical expression that described the resistivity for these electrodes was the interparticle contact radius. In addition to addressing contact geometry these expressions account for the role of space charge resistance at particle boundaries. It was found that these space charge regions can influence electrode performance at lower temperatures or for electrodes composed of smaller particles (grain size less than 1 μm).

The extended surface electrode models above primarily address charge transport across the thickness of the electrode. One exception is the work of Tanner et al. [8], who applied a two-dimensional finite difference solution to extended electrolyte structures. Deviation from one-dimensional predictions was seen for low charge transfer resistances. Similarly, Fleig and Maier [15] used finite element analysis to simulate transport in the SOFC cathode with iterated structures resembling pin fins. Regimes based on charge transfer resistance were used to define the behavior of polarization resistance and demonstrate the impact of surface morphology on performance.

A one-dimensional model for charge transport in SOFC electrodes that accounts for variable cross-section microstructure has been developed by the authors as a screening tool for more deterministically designed SOFC microstructures [16]. Based on a variable cross-section fin equation, this approach replicates experimentally observed electrode performance, including microstructural effects associated with sintering. In the present work this analytical electrochemical fin approach is compared to a two-dimensional finite element model in an effort to further establish predictive limits of the electrochemical fin approach. In most cases the simplified electrochemical fin approach provides an accurate assessment of electrode performance. In cases with reduced accuracy the one-dimensional approach predicts higher performance. This observation suggests that, when applied as a basic screening tool, the electrochemical fin approach will not produce false negative predictions of electrode performance.

2. Methodology

2.1. Analytical model

The analytical model presented is developed for an extended surface of ion conducting material, which is used to simulate connected chains of ion conducting particles that are in contact with the bulk electrolyte, illustrated in Fig. 1a. These ion conducting structures extend electrochemical activity into the electrode, away from the interface of the composite electrode and the bulk electrolyte. Thus the extended surface approach presented primarily addresses transport in the active layer of the electrode, although analyzing structures with greater lengths allows for investigation of the scale of active regions for a given microstructural geometry. Ionic transport in the electrochemically active, extended surfaces can be described using a governing equation analogous to the thermal fin equation. Therefore, the modeling approach developed is referred to as an *electrochemical fin* approach. More detailed discussion of the electrochemical fin concept and its development can be found in [16]. In this paper, periodic structures comparable to pin-fins, Fig. 1b, are considered. Extension of this approach to more complex network structures will be addressed in future work.

Several simplifying assumptions were applied in developing the electrochemical fin approach. The impacts of these assumptions upon the assessment of electrode quality that is made using the electrochemical fin approach are considered in the present work. Ionic transport is represented by a cross-sectional average potential that varies across the electrode thickness. Linear charge transfer kinetics are applied in the form of a single charge transfer resistance parameter, and charge transport is assumed to be ionic with constant potential assumed in the electronic conducting phase. Finally, space charge effects near grain boundaries are neglected in the electrochemical fin approach. These effects arise from variations in point defect concentrations associated with the establishment of thermodynamic equilibrium between the bulk of the ion conducting particle and the grain boundary [17,18]. In SOFCs, the electrolyte phase of the porous composite electrodes and the dense ion conducting ceramic electrolytes enable oxygen anion transport. Within these materials, oxygen vacancies are the primary point defect of interest. The depletion of oxygen vacancies near particle contact points and grain boundaries may lead to regions of increased resistance to charge transport [7,19]. In the porous electrodes, these space charge regions are considered to occur at interparticle contact points and near the solid-gas interface [7]. Since the space charge regions are small in comparison to the bulk ion conducting particles, they may be treated thin regions of increased resistivity, similar to a contact resistance. As demonstrated by Zhao and Virkar [7], such effects may most substantially

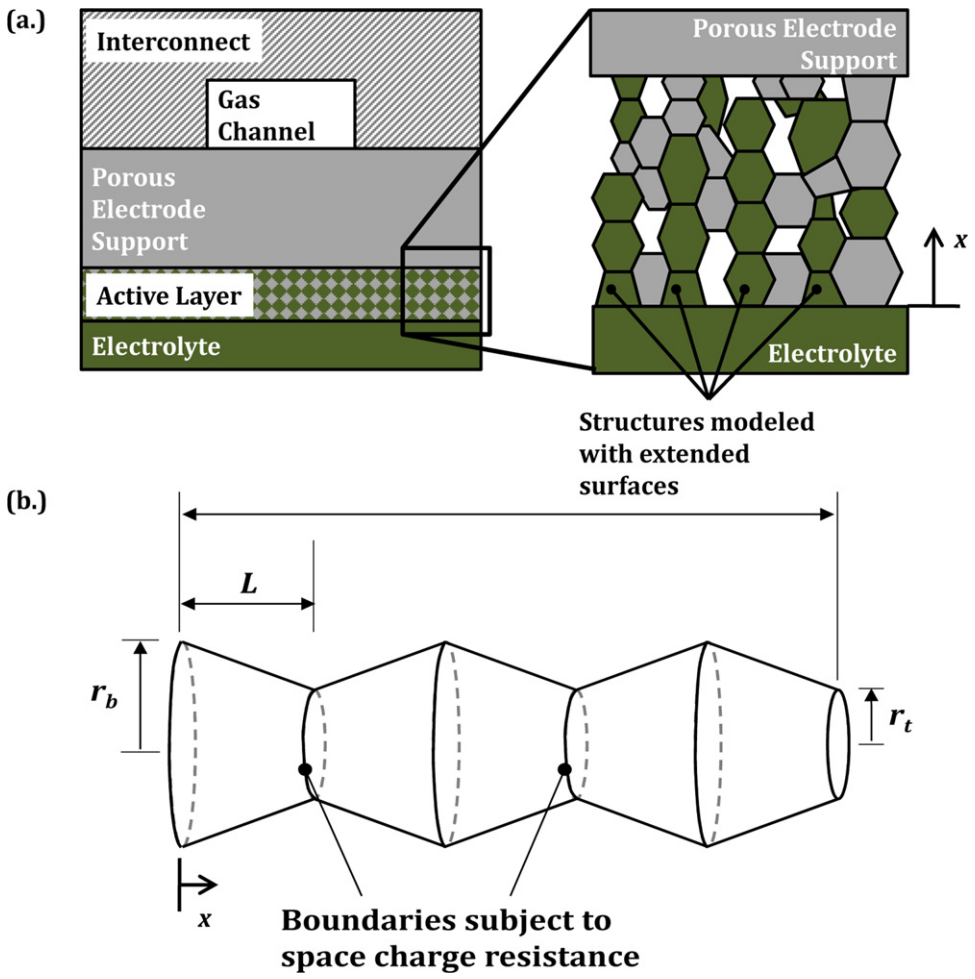

Fig. 1. The electrochemical fin approach focuses primarily on the active layer of the composite solid oxide fuel cell electrode, shown in relation to other cell components in (a). Sets of connected, ion conducting particles within the active layer of the composite electrode are simulated using an extended surface modeling approach. A periodic electrochemical fin geometry composed of iterated conical segments (b) is used to simulate these chains of connected particles that support ionic transport within the electrode. In the two-dimensional finite element model space charge effects are simulated with a contact resistance applied at the interparticle contact boundaries.

influence electrode performance at lower temperatures or for electrodes composed of smaller particles, for which the space charge region occupies a greater portion of the particle. The accuracy of describing electrical potential with a cross-sectional average and the impact of neglecting space charge regions at grain boundaries are investigated in the present work. Surface effects, inclusive of space charge resistance near the solid-gas interface, are accounted for using a charge transfer resistance term, as noted above. Therefore, the space charge effects considered are primarily associated with interparticle contact points.

SOFC analyses based on extended surface models often apply constant cross-section equations, accounting for microstructural characteristics and charge transport in a single charge transfer term [3–6,10,11]. However, implementation of this constant cross-section approach tacitly neglects the role that cross-sectional area and its variation within the microstructure play in charge transport. As implied by the results of Kenjo et al. [1,2] and demonstrated by the measurements and analysis of Zhao and Virkar [7], these variations in cross-sectional area, which result from interparticle contact geometry, can substantially affect the performance of an electrode. To account for this influence, a variable cross-section, extended surface model for electrode charge transport, outlined in Eqs. (1)–(5), has been previously developed [16]. For the case of a variable cross-section fin, the governing ordinary differential equation, Eq. (1), describes the potential difference in the electrode, as defined by Eq. (2). The solution of this variable cross-section form of the governing equation is applied as the analytical model in this work. Sintered electrode structures based on iterated units with a truncated cone (i.e., conical frustum) geometry, shown in Fig. 1b, are considered. The individual conical units have a general solution, shown in Eqs. (3)–(5), that is composed of a modified Bessel function of the first kind with order one, denoted I_1, and a modified Bessel function of the second kind with order one, denoted K_1 [20]. In this general solution C_1 and C_2 are constants to be fixed in the development of a particular solution for Eq. (1) through the application of appropriate boundary conditions at the base and the tip of the fin structure. Specific forms of these constants are provided in Appendix A for a single electrochemical fin in the shape of a conical frustum. For periodic structures, the general solutions for individual units are coupled in series and the constants, C_1 and C_2, are determined based on appropriate boundary conditions and constraints for current flow and potential. This treatment allows for flexibility in defining particle geometry, since individual segment lengths (L), base radii (r_b), and tip radii (r_t) can be varied along the length of the structure.

$$\frac{d^2\varphi}{dx^2} + \frac{1}{A_c}\frac{dA_c}{dx}\frac{d\varphi}{dx} - \frac{1}{\sigma_{io}R_{ct}A_c}\frac{dA_s}{dx}\varphi = 0 \tag{1}$$

$$\varphi(x) = V_{io}(x) - V^0 \tag{2}$$

$$\varphi[r(x)] = \frac{1}{\sqrt{r(x)}}[C_1 I_1(\beta\sqrt{r(x)}) + C_2 K_1(\beta\sqrt{r(x)})] \quad (3)$$

$$r(x) = r_b - ax \quad (4)$$

$$\beta = \sqrt{\frac{8}{\sigma_{io} R_{ct}} \frac{\sqrt{1+a^2}}{a^2}} \quad (5)$$

Non-dimensional parameters and metrics that can be used to describe the microstructure and predict the performance of an SOFC electrode have been developed from this analytical model. This development is based on four non-dimensional parameters: a normalized potential, $\varphi^* = \varphi/\varphi_b$, normalized length, $x^* = x/L_f$, and two normalized area terms, $A_s{}^* = A_s/A_{c,b}$ and $A_c{}^* = A_c/A_{c,b}$. Further details of this analysis have been provided by Nelson et al. [16]. In the present work predictions of the normalized potential and electrochemical fin efficiency are compared. The normalized potential measures the electrochemical activity of the fin structure, with a zero potential difference indicating inactivity. As in thermal fin analysis, the efficiency, η_f, is defined as the ratio of the total current conducted by the fin, i_{tot}, to the ideal current that would be conducted by a constant voltage fin held at a given base potential, φ_b, with a known charge transfer resistance, R_{ct}. This metric, defined in Eq. (6), assesses the conductive resistance within the microstructure, with a reduced efficiency indicating greater ohmic losses attributed to microstructural geometry. A similar parameter was introduced by Costamagna et al. [3] as an effectiveness factor.

$$\eta_f = \frac{i_{tot}}{(1/R_{ct})A_f \varphi_b} \quad (6)$$

2.2. Finite element model

A finite element model for charge transport was developed to determine the impacts of two-dimensional transport and space charge regions within the electrochemical fin structure. The DC electric current application of COMSOL Multiphysics served as the platform for this model. An axisymmetric two-dimensional coordinate system was applied. As in the development of the one-dimensional analytical model, surface charge transfer was characterized by a resistance term, which was incorporated into a current flux boundary condition. Space charge effects were approximated using a contact resistance boundary condition applied at the narrow junctions between iterated conical units, as illustrated in Fig. 1b. This contact resistance boundary condition was set based on a defined space charge region size and conductivity.

To confirm the validity of the contact resistance approximation for space charge effects, charge transport within a circular geometry was modeled using a two-dimensional axisymmetric finite element model with the general geometric configuration consisting of two circular particles in contact, as illustrated in Fig. 2a. Conductivity measurements taken using a DC four probe technique for porous ceria samples with a similar particle contact geometry were used to provide a basis for comparison [7]. Since these electrodes investigated demonstrated a circular particle geometry when observed using a scanning electron microscope, a similar geometry was chosen for use in this validation step. Use of this circular geometry allows for a more direct assessment of space charge effects within the microstructure. Effective conductivity predictions made by Zhao and Virkar [7] using a circular geometry were shown to agree well with experimentally observed trends for the conductivity of porous doped ceria. As in the case of the geometry illustrated in Fig. 1, space charge resistance was modeled using a contact resistance boundary condition applied between the two circular regions. Constant voltage boundary conditions were applied at either end of the structure. Following Zhao and Virkar [7], surface charge transfer effects were not incorporated. Instead, ionic conduction in the solid phase was the focus of these validation studies. The effective conductivity of the microstructure was estimated using Eq. (7), where $\bar{A}_c$ represents the average cross-sectional area of the particles in contact.

$$\sigma_{eff} = \frac{i_{tot} L_f}{\bar{A}_c (V_t - V_b)} \quad (7)$$

3. Results and discussion

The one-dimensional approach applied to modeling ionic transport within the SOFC electrode microstructure has been previously validated [16] by comparison to the experimental data of Kenjo et al. [1]. It was shown that for geometry comparable to that shown in Fig. 1, the impacts of microstructural geometry could be seen in predictions of polarization resistance. Similar geometric influence is seen in electrical potential contour plots for finite element model results for the circular particle geometry investigated in the finite element analysis (FEA) validation studies, as shown in Fig. 2b. Distortion of the current streamlines, shown in black, results from constriction of current flow within the interparticle neck region.

In Fig. 2c effective conductivity predictions made with this two-dimensional model are compared to DC conductivities measured by Zhao and Virkar [7] for a range of temperatures and oxygen partial pressures. For these studies, a particle radius of 1.25 μm was applied, with a neck radius of approximately 0.575 μm. The particle size was set to approximate the geometry considered in comparisons to experimental results made by Zhao and Virkar. The neck radius was applied as a fitting parameter in the model. This value was set to achieve conductivities in agreement with measurements taken near atmospheric conditions. The neck size was constrained to less than half of the particle size, in accordance with model limits expressed by Zhao and Virkar [7]. The space charge region was set to a size of 1.2 nm, comparable to the region encompassing the space charge layers within each particle and the grain boundary between them. The conductivities for the bulk and space charge regions, not considering geometric effects, were set as functions of temperature and oxygen partial pressure using correlations in the literature [7,21]. The finite element model provides reasonable agreement with the measurements of Zhao and Virkar taken at 600 °C and 800 °C. In both cases the model replicates trends seen in experimentally measured conductivities. Discrepancies are seen in the model predictions and experimental data for low oxygen partial pressures, with the largest disagreement seen for 800 °C. These discrepancies are best explained through the material properties applied in the finite element model. The experimental results were obtained using porous samples of samaria-doped ceria [7]. However, due to the limited availability of property data in the literature, correlations applied for estimating the bulk electron concentration and electron mobility corresponded to undoped ceria and ceria doped with materials other than samaria, primarily gadolinia. The discrepancies seen are therefore expected, particularly at low oxygen partial pressures where the influence of electronic conduction increases, and the trends predicted by the model agree with conductivity trends predicted by Zhao and Virkar using the same property correlations [7]. It should be noted that a better fit to the experimental data can be obtained by lowering the enthalpy of reaction associated with oxygen vacancy incorporation. The results shown were calculated using an oxygen vacancy incorporation reaction enthalpy of ~4.7 eV, which corresponds to undoped ceria, but the addition of dopants can reduce this reaction enthalpy and lead to the higher measured conductivity [21]. In general, the agreement between the model and experimental results suggest that approximating the space charge region with a finite contact resistance

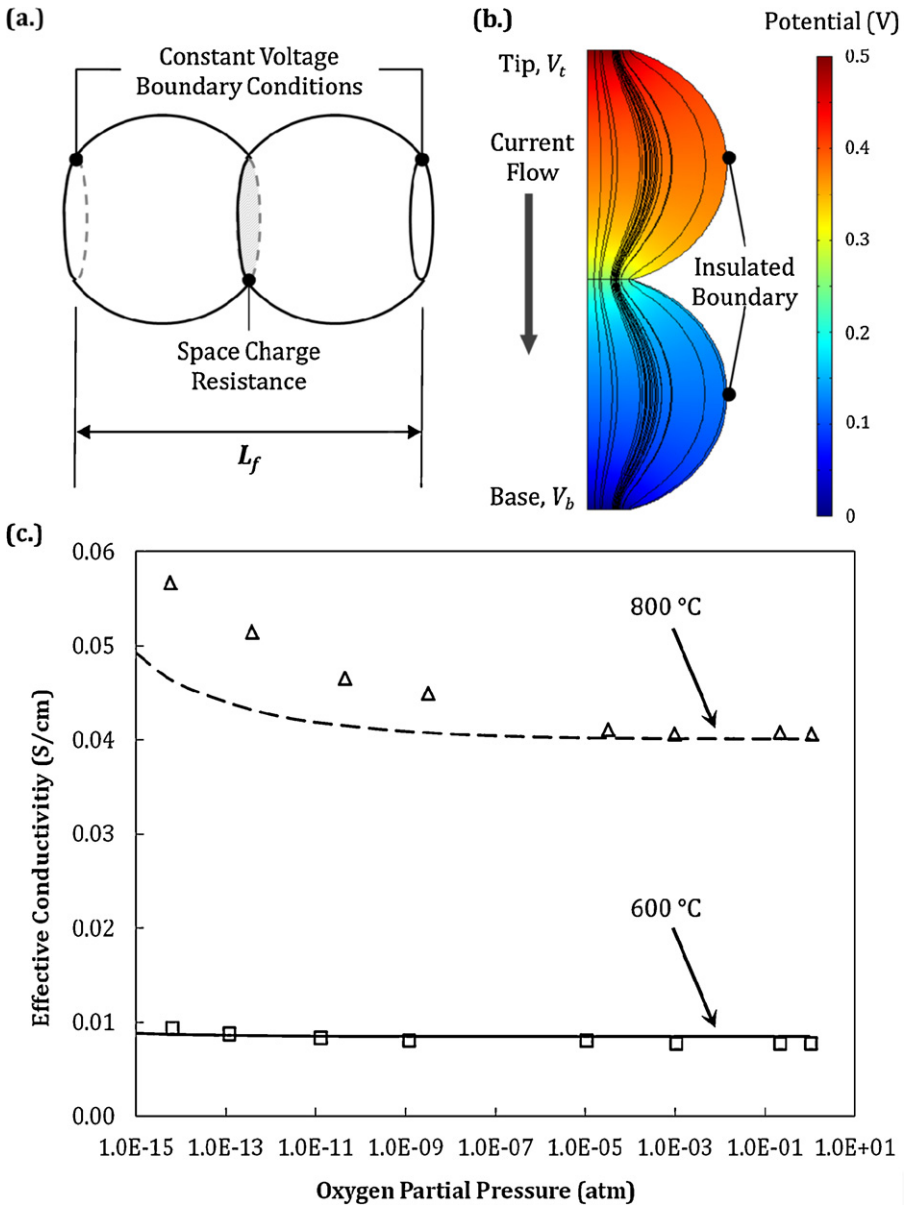

Fig. 2. A circular geometry (a) was used to test the approximation of space charge regions using a contact resistance applied at interparticle contact regions. The interparticle neck region can cause an increase in resistance related to two-dimensional charge transport effects seen in microstructural potential and current distributions (b) for the particles analyzed. The color contours represent potential and the black lines represent current streamlines. This increased resistance lowers the effective conductivity of the electrode. (c) Model predictions (lines) were found to agree well with conductivities trends measured using a DC four-probe method (symbols) [7]. (For interpretation of the references to color in this figure legend, the reader is referred to the web version of this article.)

provides a sufficient description of the effects of space charge for the microstructural geometries considered in the present work.

Parametric studies were performed to compare predictions of the analytical and finite element models, first focusing on two-dimensional transport effects. Initial comparisons were made based on predictions of the normalized potential for electrochemical fin structures of a fixed length (10 μm), which represents a common thickness of the electrochemically active region near the electrode/electrolyte interface in SOFCs [9,10,22]. Four cases were tested using a conical frustum as the iterated unit. The base radius of the conical units was set at 2 μm for all cases. Tip radii were set at 0.75 μm and 1.75 μm to simulate microstructures that would be considered poorly sintered and well sintered, respectively. Finally, lengths of 0.25 μm and 2 μm were considered for the iterated segments. This set of geometries serves as the basis for all comparisons of the analytical and finite element models.

Results of these initial parametric studies are shown in Fig. 3 for a well sintered geometry with a segment length of 2 μm and for the two poorly sintered geometries. For the finite element results the potential corresponds to the value along the fin centerline. The well sintered case, Fig. 3a, shows minimal influence of two-dimensional transport, as indicated by the agreement between to analytical and finite element solutions. This agreement was seen for both well sintered cases, and the cross-sectional average of the potential, plotted along the fin structure, was found to be equal to the centerline value in these cases. The poorly sintered predictions of the analytical model clearly deviate from the finite element solutions, as shown in Fig. 3b and c. Significant variation is seen along the fin length for the poorly sintered geometry with a 2 μm segment length, Fig. 3b. The apparent oscillation along the fin length can be attributed to the cross-sectional geometry influencing the flow of current. For tapered regions near the points representing

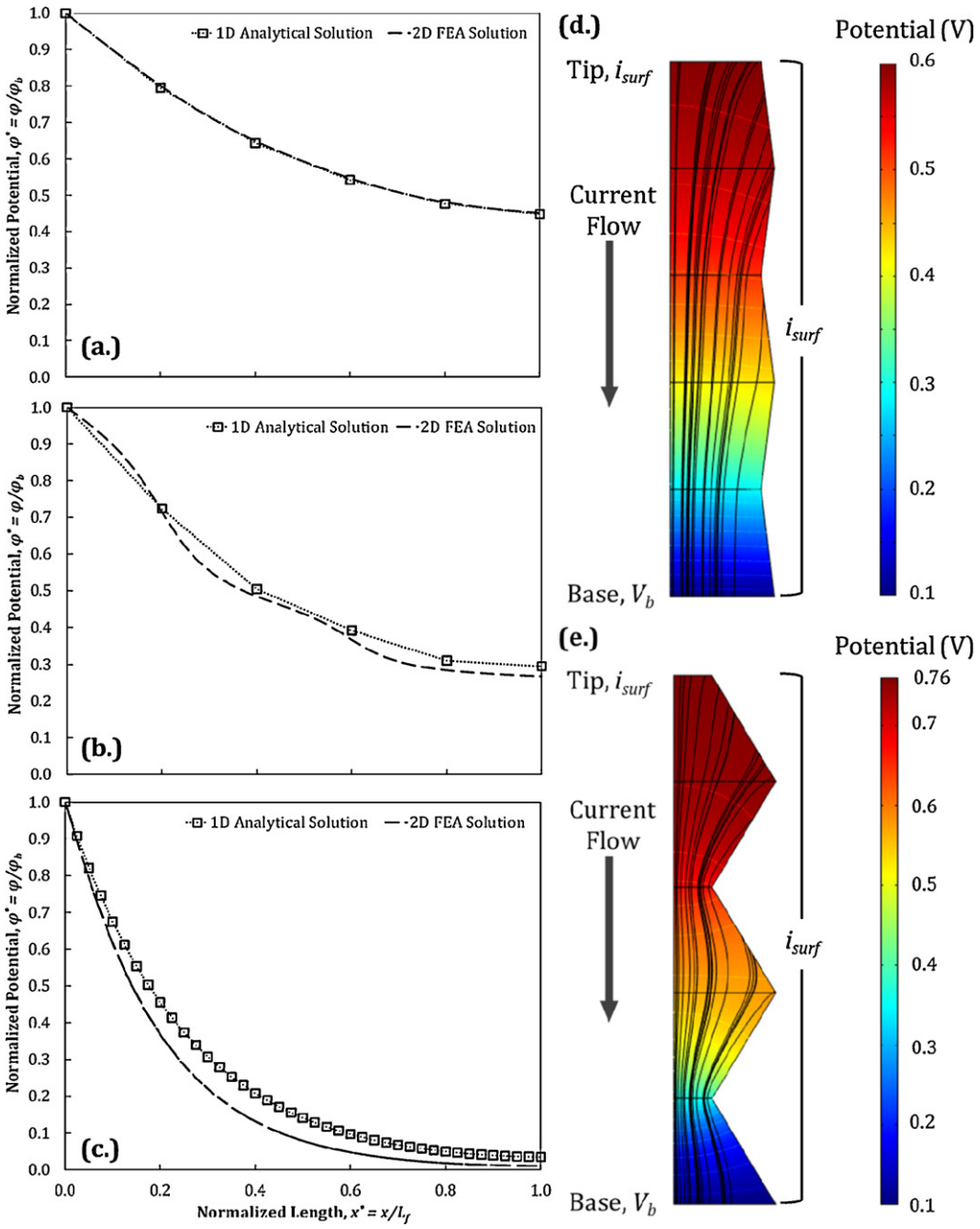

Fig. 3. Normalized potential distributions calculated with the 1D analytical model and 2D FEA model for electrochemical fin structures: (a) well sintered (r_{tip} = 1.75 μm) with 2 μm base radius and segment length (b) poorly sintered (r_{tip} = 0.75 μm) with 2 μm base radius and segment length (c) poorly sintered (r_{tip} = 0.75 μm) with 2 μm base radius and 0.25 μm segment length. The two-dimensional potential and current distributions calculated with the finite element model are shown for the (d) well sintered and (e) poorly sintered cases with a 2 μm segment length. The color contours represent potential and the black lines represent current streamlines. (For interpretation of the references to color in this figure legend, the reader is referred to the web version of this article.)

interparticle contacts (x^* = 0.2 and 0.6), a sharp drop in the normalized potential is caused by increased resistance related to the constriction of the current flow. The current then spreads as the particle broadens, which facilitates current flow and causes a less pronounced potential gradient in the widest regions of the particles (x^* = 0.4 and 0.8). This behavior can be seen when comparing potential and current distributions for the geometries related to the normalized potentials plotted in Fig. 3a and b. Compared to its well sintered counterpart, described by Fig. 3a and d, the poorly sintered geometry, described by Fig. 3b and e, shows significant constriction of the current flow. However, while the exact profiles for the analytical and finite element predictions do not coincide, the analytical prediction for the poorly sintered case does track the trend of the structure reasonably well, suggesting that the analytical approach may provide a sufficient approximation in this case. This agreement is not seen for the poorly sintered case shown in Fig. 3c. Thus the analytical approach is not expected to be sufficient in this final case.

Further comparison of the analytical and finite element models was made in terms of the fin efficiency. Predictions of this metric are compared over a range electrode thicknesses in Fig. 4. The geometries representing well sintered electrodes are shown in Fig. 4a, and poorly sintered geometries are shown in Fig. 4b. As noted and further illustrated in Fig. 4a, the one-dimensional model provides an accurate prediction of electrode performance for well sintered electrodes. For the poorly sintered cases, agreement in the predictions

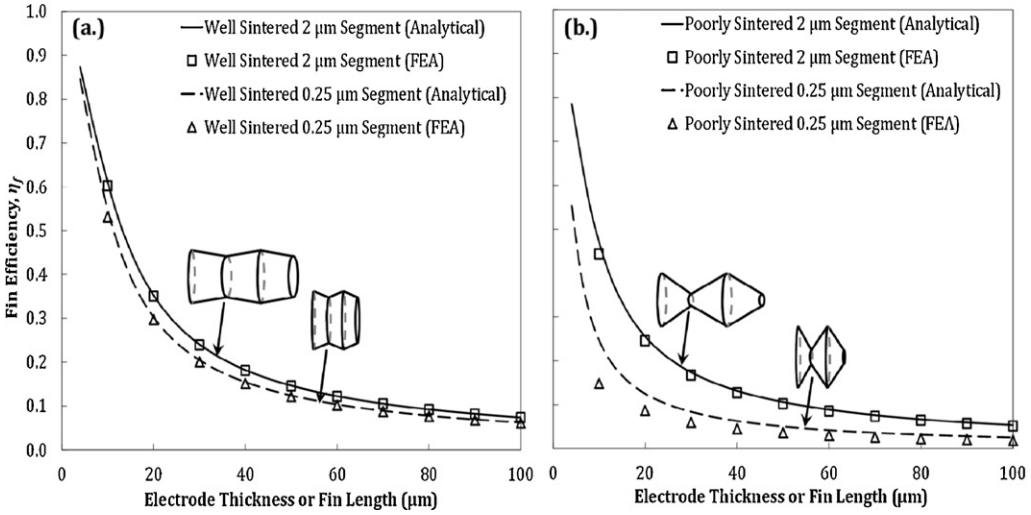

Fig. 4. Fin efficiency as function of total electrode thickness for electrochemical fin structures representing (a) well sintered and (b) poorly sintered geometries. Lines represent 1D analytical model predictions and symbols represent 2D finite element model predictions.

is maintained for the case with a 2 μm segment length. This agreement stems from the fact that the two models predict comparable base currents, which is instrumental in calculating the fin efficiency. For the final case, a poorly sintered geometry with a 0.25 μm segment length, the constriction of current flow within the structure increases ohmic losses significantly beyond the level accounted for in the analytical model. In such cases the electrochemical fin model over predicts performance and may not be considered as a sufficient description of transport for more rigorous analyses. However, this approach may still be worthwhile as a basic screening tool in such cases. That is, a microstructural geometry found to be lacking by the fin approach would not be expected to show improved performance when modeled in further geometric detail.

The effects of additional resistance from space charge regions around interparticle contacts were also considered for the geometric cases analyzed above. Two sizes of the space charge regions were modeled in these studies: 1 nm and 10 nm. These sizes were selected to represent small and large space charge regions based on sizes estimated in the literature [19]. For the present studies, a conductivity of 0.05 S m^{-1} was applied for both of these regions. This value was chosen to be comparable in magnitude to space charge conductivity noted by Zhao and Virkar for operation at 800 °C [7].

Analytical and finite element predictions of the fin efficiency taken from the space charge studies for geometries based on a 0.25 μm segment length are shown as a function of the resistivity ratio in Fig. 5. The resistivity ratio measures the relative size of ionic and charge transfer resistivity in the electrode and is defined based on the coefficient of the third term on the left-hand side of Eq. (1). Details of its derivation can be found in [16]. The 0.25 μm segment length is considered because the influence of space charge resistance on the structures based on a 2 μm segment length was found to be significantly less pronounced, a trend that agrees with the resistivity predictions of Zhao and Virkar [7]. Specifically, as the particle size increases the additional resistance from the space charge region contributes less to the total resistance of the structure because there are fewer space charge regions within the structure and their length relative to the larger particles is smaller.

Efficiency predictions for a relatively narrow 1 nm space charge region are shown in Fig. 5a, and predictions for a wider 10 nm space charge region are shown in Fig. 5b. Analytical model predictions are shown with lines and finite element predictions are shown with symbols. Cases with and without space charge effects are considered for the finite element models to discern the

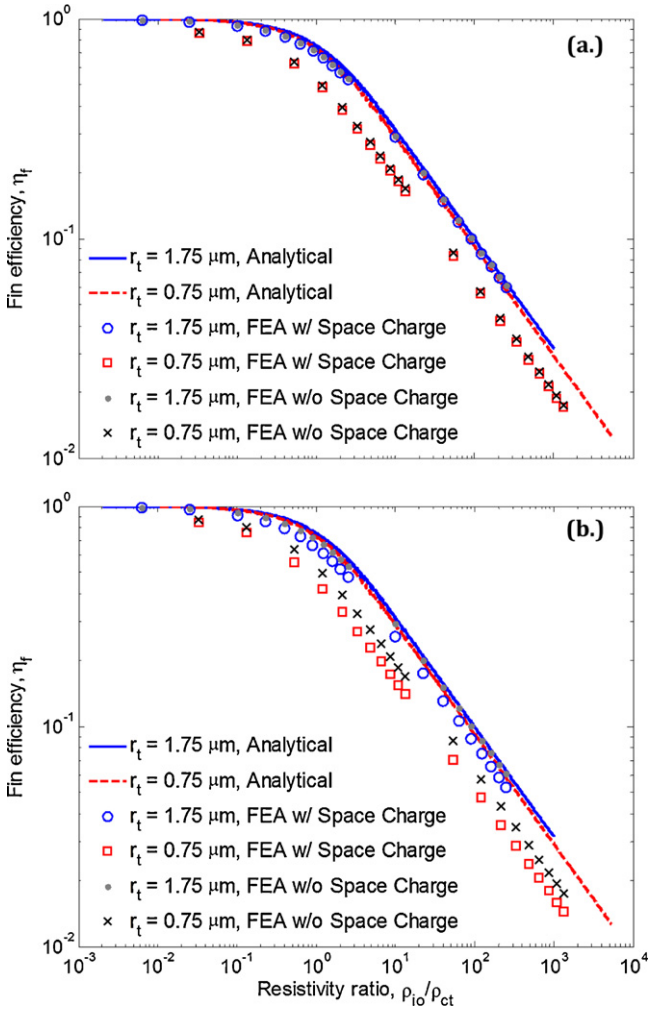

Fig. 5. Comparison of fin efficiency predicted as a function of resistivity ratio by the analytical model (lines) and finite element model (symbols). Finite element predictions include cases with and without space charge regions considered at interparticle contacts. Two different space charge regions width are shown (a) 1 nm and (b) 10 nm.

influence of two-dimensional transport to relative space charge effects. The most distinct deviation from the analytical predictions is found for the poorly sintered geometries, where the finite element solutions predict much lower fin efficiencies. This discrepancy becomes more pronounced as ionic conduction begins to dominate transport ($\rho_{io}/\rho_{ct} > 1$). This difference between the analytical and finite element predictions may be attributed to two-dimensional transport within the structure or space charge resistance. The relative contribution of these two effects can be determined by comparing finite element results with and without the space charge regions included. For the case of a relatively narrow space charge region, efficiencies were at most ~3% higher when not including space charge resistance. Thus, the primary source of disagreement between the analytical and finite element approaches is due to two-dimensional transport effects. For the 10 nm case, this discrepancy ranged from 3% to 21%, suggesting a more significant role for the effects of space charge regions. As seen in the cases based on the 2 μm segment length, the reduced influence of the narrow space charge region can be attributed to the smaller length of the space charge region relative to the particle size.

When comparing the analytical and finite element models, without consideration of space charge effects, it was found that the merit of the electrochemical fin approach as a basic screening tool was not compromised. A microstructure demonstrating lower performance as predicted analytically would still show poor performance under more rigorous analysis. This trend is also seen when incorporating the effects of space charge regions on ionic transport. In general greater error was seen for geometries that would be considered poorly sintered, and this error increased primarily for cases exhibiting lower fin efficiencies that indicate poor electrode performance. This finding further confirms the capabilities of the electrochemical fin approach as a basic design tool in developing next generation SOFC electrode microstructures.

4. Conclusions

An analytical model for charge transport within the SOFC electrode microstructure has been developed using an approach similar to thermal fin analysis. It has been previously demonstrated that this model accounts for variable cross-section solid geometry and replicates experimentally observed behavior related to SOFC electrode microstructure. However, the performance impacts of extreme cross-sectional variation and space charge regions within the microstructures were not addressed in detail in this model's development. These issues have been addressed in the present work using a two-dimensional, axisymmetric finite element model for the extended surface geometries that was developed to simulate SOFC electrode microstructure inclusive of space charge effects that arise in interparticle contact regions.

Microstructural geometries simulated by periodic structures composed of iterated base units with a conical geometry were investigated using this one-dimensional analytical model. The predictions of the one-dimensional model were compared to the axisymmetric two-dimensional finite element model, with and without space charge resistance. For most of the geometries considered the electrochemical fin approach was found to provide an accurate prediction of electrode performance. Effects of two-dimensional transport within the structures examined were found to influence predictions of normalized potential for cases with narrow contact points between iterated segments, representative of a poorly sintered electrode microstructure. However, for larger particle sizes, the analytical predictions provided a sufficient approximation of electrode performance in terms of the fin efficiency. This was not the case for smaller particle sizes. For geometries representing well sintered electrode microstructures relatively wide space charge regions were found to exert additional influence over performance for smaller particle sizes. Within the set of poorly sintered geometries these wider space charge regions were found to influence performance predictions to a greater degree.

The more rigorous modeling of transport within the electrode microstructure revealed limitations of the analytical electrochemical fin approach. A clear trend of performance over prediction by the analytical model was seen when examining its discrepancies with respect to finite element model predictions. However, this trend does not necessarily detract from the applicability of the electrochemical fin approach as a design tool for SOFC electrodes. Microstructures showing poor performance based on the analytical model are not expected to show improved performance when considering the effects of two-dimensional transport or space charge regions at interparticle contact points. Thus, application of the electrochemical fin approach is warranted as a means of focusing more detailed modeling efforts that may be applied in the development of novel SOFC electrode microstructures.

Acknowledgments

Financial support from an Energy Frontier Research Center on Science Based Nano-Structure Design and Synthesis of Heterogeneous Functional Materials for Energy Systems (HeteroFoaM Center) funded by the U.S. Department of Energy, Office of Science, Office of Basic Energy Sciences (Award DE-SC0001061) is gratefully acknowledged. The authors are grateful to Prof. Anil V. Virkar at the University of Utah for invaluable discussions on SOFC microstructure and conductivity measurements.

Appendix A.

The particular solutions that comprise the electrochemical fin model can be determined through the application of appropriate boundary conditions. At the base of the fin structure ($x = 0$), two types of boundary conditions are considered: (*i*) constant potential base (Eq. (A1)) and (*ii*) constant current base (Eq. (A2)). These boundary conditions can be applied to Eq. (3) to first obtain the constant C_2. This constant is defined in Eqs. (A3) and (A4) for the constant potential case and constant current case, respectively. For the modified Bessel functions I_n and K_n the subscript denotes the order of the function.

$$\varphi(0) = \varphi_b \tag{A1}$$

$$\left.\frac{d\varphi}{dx}\right|_{x=0} = -\frac{i_{tot}}{A_b\sigma_{io}} \tag{A2}$$

$$C_2 = \frac{\varphi_b\sqrt{r_b} - C_1 I_1(\beta\sqrt{r_b})}{I_1(\beta\sqrt{r_b})} \tag{A3}$$

$$C_2 = \frac{-(i_{tot}/A_b\sigma_{io}) - C_1[(a/r_b^{3/2})I_1(\beta\sqrt{r_b}) - (\beta a/2r_b)I_0(\beta\sqrt{r_b})]}{(a/r_b^{3/2})K_1(\beta\sqrt{r_b}) + (\beta a/2r_b)K_0(\beta\sqrt{r_b})} \tag{A4}$$

$$\beta = \sqrt{\frac{8}{\sigma_{io}R_{ct}}\frac{\sqrt{1+a^2}}{a^2}} \tag{A5}$$

With the constant C_2 determined, the constant C_1 can be found using the boundary conditions at the tip of the fin structure ($x = L_f$). Two types of boundary conditions are considered in this case: (*i*) insulated tip (Eq. (A6)) and (*ii*) active tip (Eq. (A7)). The first of these conditions is commonly applied to account for a current collecting interconnect that blocks the flow of ions. The second would account for an electrochemically active structure connected to the electrolyte and in contact with percolating electronic conductor

and pore phases. A constant potential case may also be derived. However, this case would preclude blocking of ionic current at the cell interconnect, and is therefore considered less relevant for fuel cell electrodes.

$$\left.\frac{d\varphi}{dx}\right|_{x=L_f} = 0 \tag{A6}$$

$$-\sigma_{io}\left.\frac{d\varphi}{dx}\right|_{x=L_f} = \frac{1}{R_{ct}}\varphi(L_f) \tag{A7}$$

Combining the constant potential base condition with the insulated tip condition, the constant C_1 is found to take the form of Eq. (A8). Similarly, for a constant potential base and active tip C_1 takes the form of Eq. (A9).

$$C_1 = \frac{\varphi_b\sqrt{r_b}\cdot[K_1(\beta\sqrt{r_t})/\sqrt{r_t}+(\beta/2)K_0(\beta\sqrt{r_t})]}{\begin{array}{l} I_1(\beta\sqrt{r_b})\cdot[K_1(\beta\sqrt{r_t})/\sqrt{r_t}+(\beta/2)K_0(\beta\sqrt{r_t})] \\ -K_1(\beta\sqrt{r_b})\cdot[I_1(\beta\sqrt{r_t})/\sqrt{r_t}+(\beta/2)I_0(\beta\sqrt{r_t})]\end{array}} \tag{A8}$$

$$C_1 = \varphi_b\sqrt{r_b} \times \left[I_1(\beta\sqrt{r_b}) - \frac{\begin{array}{c}[(r_t/a\sigma_{io}R_{ct})I_1(\beta\sqrt{r_t})+I_1(\beta\sqrt{r_t}) \\ -(\beta\sqrt{r_t}/2)I_0(\beta\sqrt{r_t})]K_1(\beta\sqrt{r_b})\end{array}}{(r_t/a\sigma_{io}R_{ct})+K_1(\beta\sqrt{r_t})+(\beta\sqrt{r_t}/2)K_0(\beta\sqrt{r_t})}\right]^{-1} \tag{A9}$$

For the case of a fixed current applied at the base of the structure (Eq. (A2)) the expressions for the constants are more complicated. Thus it is convenient to define several functions, Eqs. (A10)–(A13). These functions help simplify the expressions for C_1.

$$f_1(r) = \frac{a}{r^{3/2}}I_1(\beta\sqrt{r}) - \frac{\beta a}{2r}I_0(\beta\sqrt{r}) \tag{A10}$$

$$f_2(r) = \frac{1}{r^{3/2}}K_1(\beta\sqrt{r}) + \frac{\beta}{2r}K_0(\beta\sqrt{r}) \tag{A11}$$

$$g_1(r) = \left[\frac{a}{r}K_1(\beta\sqrt{r}) + \frac{\beta a}{2\sqrt{r}}K_0(\beta\sqrt{r})\right] \tag{A12}$$

$$g_2(r) = \left[\frac{a}{r}I_1(\beta\sqrt{r}) + \frac{\beta a}{2\sqrt{r}}I_0(\beta\sqrt{r})\right] \tag{A13}$$

With these functions defined, expressions for C_1 can be cast for the cases of a constant base current with an insulated tip and an active tip. These forms of the constant C_1 are given in Eqs. (A14) and (A15), respectively.

$$C_1 = \frac{(i_{tot}/A_b\sigma_{io})f_2(r_t)}{f_1(r_t)\cdot f_2(r_b) - f_1(r_b)\cdot f_2(r_t)} \tag{A14}$$

$$C_1 = \frac{\begin{array}{l}(i_{tot}R_{ct}/A_b)g_1(r_t)+(i_{tot}/A_b\sigma_{io})K_1(\beta\sqrt{r_t}) \\ af_2(r_b)\cdot[I_1(\beta\sqrt{r_t})-K_1(\beta\sqrt{r_t})] \\ -\sigma_{io}R_{ct}[f_1(r_b)\cdot g_1(r_t) - af_2(r_b)\cdot g_2(r_t)]\end{array}}{}$$ (A15)

References

[1] T. Kenjo, S. Osawa, K. Fujikawa, J. Electrochem. Soc. 138 (1991) 349–355.
[2] T. Kenjo, M. Nishiya, Solid State Ionics 57 (1992) 295–302.
[3] P. Costamagna, P. Costa, V. Antonucci, Electrochim. Acta 43 (1998) 375–394.
[4] P. Costamagna, P. Costa, E. Arato, Electrochim. Acta 43 (1998) 967–972.
[5] S. Sunde, J. Electrochem. Soc. 143 (1996) 1930–1939.
[6] S. Sunde, J. Electrochem. Soc. 143 (1996) 1123–1133.
[7] F. Zhao, A.V. Virkar, J. Power Sources 195 (2010) 6268–6279.
[8] C.W. Tanner, K. Fung, A.V. Virkar, J. Electrochem. Soc. 144 (1997) 21–30.
[9] H. Zhu, R.J. Kee, J. Electrochem. Soc. 155 (2008) B715–B729.
[10] M. Cannarozzo, S. Grosso, G. Agnew, A. Del Borghi, P. Costamagna, J. Fuel Cell Sci. Technol. 4 (2007) 99–106.
[11] S. Sunde, J. Electroceram. 5 (2000) 153–182.
[12] J.H. Nam, D.H. Jeon, Electrochim. Acta 51 (2006) 3446–3460.
[13] L.C.R. Schneider, C.L. Martin, Y. Bultel, D. Bouvard, E. Siebert, Electrochim. Acta 52 (2006) 314–324.
[14] L.C.R. Schneider, C.L. Martin, Y. Bultel, L. Dessemond, D. Bouvard, Electrochim. Acta 52 (2007) 3190–3198.
[15] J. Fleig, J. Maier, J. Eur. Ceram. Soc. 24 (2004) 1343–1347.
[16] G.J. Nelson, A.A. Peracchio, W.K.S. Chiu, J. Power Sources 196 (2011) 4695–4704.
[17] K. Lehovec, J. Chem. Phys. 21 (1953) 1123–1128.
[18] A. TSchope, Solid State Ionics 139 (2001) 267–280.
[19] X. Guo, J. Maier, J. Electrochem. Soc. 148 (2001) E121–E126.
[20] M. Abramowitz, I.A. Stegun, Handbook of Mathematical Functions: With Formulas, Graphs, and Mathematical Tables, U.S. Dept. of Commerce, National Bureau of Standards, Washington, DC, 1970.
[21] H.L. Tuller, in: O.T. Sorensen (Ed.), Nonstoichiometric Oxides, Academic Press, New York, 1981, p. 271.
[22] J. Kim, A.V. Virkar, K. Fung, K. Mehta, S.C. Singhal, J. Electrochem. Soc. 146 (1999) 69–78.